Performance Analysis of Intelligent Reflecting Surface-Aided Decode-and-Forward UAV Communication Systems

Osamah S. Badarneh, *Member, IEEE*, Mohamad K. Awad, *Senior Member, IEEE*
Sami Muhaidat, *Senior Member, IEEE*, and Fares S. Almehmadi

***Abstract*—In this paper, we consider a scenario of a decode-and-forward (DaF) wireless system supporting the communication of an unmanned aerial vehicle (UAV) with a ground-control-station (GCS) through an intelligent reflecting surface (IRS). Particularly, the UAV moves according to the three-dimensional (3D) random way point model at low altitude in a complex urban environment. However, a stationary relay-station (RS) decodes and forwards the UAV's signal over an IRS-aided virtual line-of-sight (LoS) link to a GCS. The highly dynamic and terrain-dependent UAV-to-RS channel follows the Beaulieu-Xie fading model. However, the RS-to-IRS and IRS-to-GCS links enjoy clear LoS; thus, follow the Rice fading model. We derive closed-form new expressions for the probability density functions (PDFs) and the cumulative distribution functions (CDFs). Then based on the derived statistical expressions, several performance metrics including outage probability, average bit error rate, and ergodic channel capacity are derived in closed-forms. Additionally, simple and accurate approximated expressions in the high signal-to-noise ratio regime are also provided. The analytical results are validated through some representative numerical examples and supported by Monte-Carlo simulation results.**

***Index Terms*—IRS, RWP mobility, UAV.**

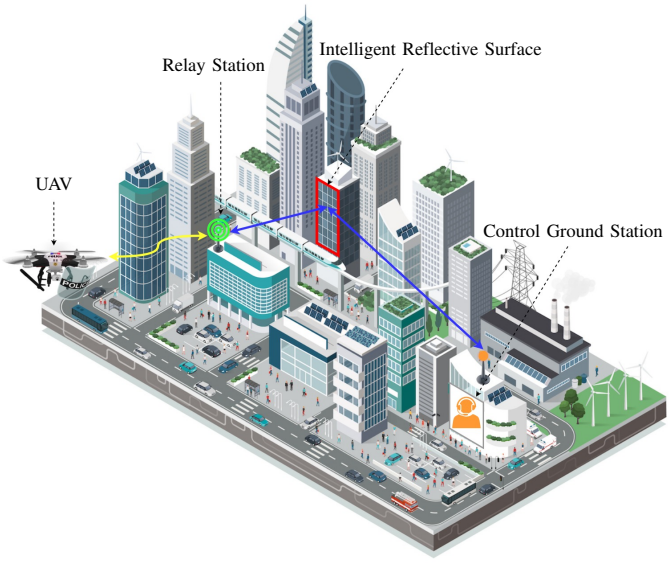

Fig. 1. An illustration of IRS-Aided DaF UAV Communication System.

I. Introduction

The upsurge in unmanned aerial vehicles (UAVs) applications in various market segments such as military, commercial, law enforcement, government, and consumer drives a compound annual growth rate (CAGR) of 15.5% in the UAV market from 2019 to 2025. Starting at an estimate of USD 19.3 billion in 2019, the UAV market size is projected to reach USD 45.8 billion by 2025 [1]. The full exploitation of the anticipated market growth demands the satisfaction of numerous application-related stringent design requirements. One common requirement among all applications is reliable communication to support remote control and mission-related data delivery. However, UAV applications across all market segments may require low-altitude flight operations in urban or semi-urban environments. For instance, military forces take advantage of UAV flexibility and maneuverability to support urban war-fighting capabilities by aerial scanning of buildings to identify and track enemy threats, besides detecting mines and weapons [2]. The commercial UAVs applications include but are not limited to remote sensing, filming, and smart logistics [3]. UAVs provide law enforcement with the necessary tools to operate with greater safety when responding to an active shooting or armed hostage situation. Furthermore, it facilitates a safe tracking of vehicles and suspects in highly populated urban areas. Governmental organizations such as disaster–response and emergency–management agencies have utilized UAVs for search and rescue missions in post-disaster situations. Tasks such as aerial photo mapping, roof-top observation, fast indoor inspection, post-disaster area exploration, evacuation of a trapped fire crew, and aerial surveillance can easily be accomplished by UAVs [4], [5]. UAVs have also been widely adopted to support consumers' entertainment-related applications like aerial photography, gaming, and hobbyist purposes [6].

Operating at low-altitude in an urban environment where buildings' height is significantly larger than the UAV's altitude, the Line-of-Sight (LoS) link between the UAV and a remote ground–control–station (GCS) is likely to be blocked or severely deteriorated [7], [8]. This has a devastating impact on UAVs communication, especially in delay-sensitive and loss-intolerant applications, such as those mentioned above. Therefore, the architectural design of the communication system connecting UAVs to a remote GCS must be revisited to realize a virtual LoS communication, thereby enabling real-time control and facilitating critical data delivery. To this end, we propose the utilization of a decode-and-forward (DaF)-based relay-

O. S. Badarneh is with the Electrical and Communication Engineering Department, School of Electrical Engineering and Information Technology, German-Jordanian University, Amman 11180, Jordan (e-mail: osamah.badarneh@gju.edu.jo).

M. K. Awad is with the Computer Engineering Deportment, College of Engineering and Petroleum, Kuwait University, Kuwait (e-mail: mohamad@ieee.org).

S. Muhaidat is with the Center for Cyber-Physical Systems, Department of Electrical Engineering and Computer Science, Khalifa University, Abu Dhabi 127788, UAE, and also with the Department of Systems and Computer Engineering, Carleton University, Ottawa, ON K1S 5B6, Canada (e-mail: muhaidat@ieee.org).

F. S. Almehmadi is with the Electrical Engineering Department, University of Tabuk, Tabuk, 71491, Saudi Arabia, (email: fal_mehmadi@ut.edu.sa).

station (RS) to uplift the UAV signal to a sufficiently high altitude, such that it can be reflected by an LoS-accessible intelligent reflective surface (IRS) to a distant GCS as shown in Fig. 1.

IRS, also known as reconfigurable intelligent surfaces (RIS), are surfaces made up of many passive elements with electronically configurable electromagnetic properties, i.e., reflection, refraction and absorption [9]. These properties can be configured to steer signals via passive beam-forming towards an intended receiver via a path that bypasses the LoS-blocking obstacles. Whereas the DaF RS decodes, re-modulates, and transmits relayed signals, the IRS reflects the impinging signals on its passive elements by tunning their phase shifts, so they add constructively at the receiver [9], [10]. The constructive addition of signals generates a strong signal and alleviates the multipath effect, enhancing the achievable data rate. Furthermore, IRS offers significant coverage extension with minimal energy consumption, minimal computational power, and minimal signal processing, as quantitatively demonstrated in [11]. A comprehensive analysis of numerous use-cases considering the joint application of UAV and IRS technologies for future wireless communication networks was recently presented in [12]. In [8], the authors investigated the joint UAV trajectory and IRS passive beam-forming design to maximize an IRS-assisted UAV downlink channel's average achievable rate. In [13], the authors investigated the optimal placement of IRS to support ground-to-air UAVs communications. The IRS technology was applied in [14] to secure the communication between a UAV and a ground user in the presence of an eavesdropper.

Being comprised of passive elements of low energy consumption that do not require a transmission module to reflect signals makes IRS energy-efficient and cost-effective [8]. This opens the door wide for a large-scale deployment of IRS on walls and roofs of buildings, lampposts, and billboards in future smart cities [15]. Similarly, dense deployment of relays and distributed remote radio heads (RRH) is intrinsic to future smart cities [15]. The integration of relays and IRSs in future smart cities offers an unprecedented opportunity to turn an uncontrollable wireless channel into a configurable software-defined medium. The software-defined channel characteristics are optimized to enable ultra-reliable connectivity for UAVs' real-time control and ultra-low-latency mission-critical data delivery.

Several recent efforts have recognized the potential of integrating RS and IRSs for UAV communication. In [16], the authors considered a scenario in which a UAV decodes-and-forwards a ground-sourced signal, reflected by an IRS, to a ground destination. The authors assume that the ground-to-IRS channel is Rayleigh; whereas, the IRS-to-UAV and UAV-to-ground channels are assumed Rician. They developed a framework for analyzing the average bit-error rate (BER), average capacity and outage probability. Results therein confirm the effectiveness of IRSs in enhancing coverage and reliability of UAV communication systems. Considering a different scenario, the authors in [17], [18] used IRS in the mixed, free-space optical (FSO) and radio frequency (RF), relay communication systems. The reported results demonstrate that this integration can significantly improve the outage and BER performance in FSO-RF communication systems. This integration has also been recently studied in dual-hop mixed RF and underwater wireless optical communication systems [19], [20], where outage, BER, and diversity performance improvement was demonstrated. The IRS does not necessarily mediate the source–and–relay or relay–and–destination. On the contrary, IRS can be utilized at the source [21] or at both the source and relay [22] to enhance the quality of transmitted signals in the presence of severe interference. The outage probability analysis presented in [22] and [21] confirmed the IRS's impact in mitigation of interference at the relay.

Although the existing works have provided deep insights into the performance of integrating DaF RSs and IRSs in various application scenarios, the effectiveness of this integration to aid transmissions of UAVs operating at low altitudes has not been considered yet. Motivated by the research trends mentioned above and the recent prevalence of low-altitude UAV missions, we aim to fill this vital research gap. Mainly, assuming a three-dimensional (3D) random way point mobility model of the UAV and realistic channels assumptions, we investigate the system's performance in terms of outage probability, BER, and channel capacity. The channel between the UAV and the RS consider the multi-path components as well as the line-of-sight component, which follows the Beaulieu-Xie fading model. Whereas, the channels between the RS and the IRS, and between the IRS and the GCS follow the Rice fading model.

It is important to mention that the system model in [16] is different than the one considered in this work; First, in the considered system, the source is a mobile UAV operating in a hostile wireless environment; however, in [16], the source is a stationary ground user. Second, the RS in the considered system is stationary; whereas, the RS in [16] is a UAV operating at high altitudes. Third, the channel assumptions in [16] match the system model considered therein, but not the model considered in this work. Therefore, it is not possible to apply the results presented in [16] to analyze the performance of the system under consideration. Our key contributions in this work can be summarized as follows:

- The PDFs and the CDFs for a DaF IRS-aided UAV communication system are derived in closed-form, considering UAV 3D mobility and realistic channel models.
- Several useful performance metrics such as the outage probability, average BER, and ergodic channel capacity are derived in closed-form.
- To gain more insights into the analytical results, simple and accurate approximated expressions in the high SNR regime are obtained. Additionally, an accurate approximated expression for the ergodic channel capacity is also obtained for the low SNR regime.

The remainder of this paper is organized as follows. In Sec. II, the system and channel models are presented. In Sec. III, we derived statistical expressions, i.e., the PDFs and the CDFs, for the system under consideration. Also, closed-form analytical expressions for the outage probability, average BER, and ergodic channel capacity are derived in Sec. III. To gain insights into our analysis, in Sec. IV, we derive simple and

accurate approximated expressions in the high SNR regime for the derived performance metrics. Discussion on numerical and Monte-Carlo simulation results are provided in Sec. V. Finally, conclusions are drawn in Sec. VI.

II. System and Channel Models

Consider the wireless communication system shown in Fig. 1. In this system, data transmission is accomplished through two time slots. In the first time slot, the UAV transmits data to the RS over the first hop. Subsequently, i.e., during the second time slot, the RS decodes the received signal and then forwards it to the destination with the aid of an IRS over the second hop. Thus, the received signal at RS can be given as

$$y_1 = \sqrt{\frac{P_t}{r^{\alpha}}} h x + n_1, \tag{1}$$

where P_t is the power transmitted by the UAV, x denote the transmitted signal, n_1 an additive Gaussian noise with zero mean and variance $\sigma^2_{n_1}$, and the path-loss exponent is denoted by α. The distance between the UAV and the RS is random and denoted by the random variable (RV) r. Here, we assume that the RV r follows the 3D random waypoint model (RWP). In 3D topology RWP model, the RS is assumed to be located at the center of a sphere with a maximum radius of D. As such, the PDF of the UAV-RS distance r is given by

$$f_R(r) = \sum_{\ell=1}^{n} \frac{B_\ell}{D^{\beta_\ell+1}} r^{\beta_\ell}, \qquad 0 \le r \le D, \tag{2}$$

where $n = 3$, $B_\ell = \frac{1}{72}[735, -1190, 455]$, and $\beta_\ell = [2, 4, 6]$ [23].

The wireless channel between the UAV and the RS, denoted by h, is modeled by the Beaulieu-Xie fading model. Hence, the PDF of the received signal envelope is given by [24]

$$f_X(x) = A\, x^m \exp\left(-\frac{m}{\Omega} x^2\right) I_{m-1}\left(\frac{2m\lambda}{\Omega} x\right), \tag{3}$$

in which $A = \left(\frac{2m}{\Omega}\right) \frac{\exp\left(-\frac{m}{\Omega}\lambda^2\right)}{\lambda^{m-1}}$, m represents the number of multi-paths, λ^2 is the power of the line-of-sight (LoS) components, while the power of the NLoS is denoted by $\Omega = \mathbb{E}[X^2]$, whereby $\mathbb{E}[\cdot]$ is the expectation operator. $I_\nu(\cdot)$ is the ν-th order modified Bessel function of the first kind [25, Eq. (8.445)]. Note that the Beaulieu-Xie fading models include other well-known distributions as special cases, such as Rice ($m = 1$) and Nakagami-m ($\lambda \to 0$).

The received signal at the destination can be expressed as

$$y_2 = \sqrt{\frac{P_s}{d_1^{\alpha_1} d_2^{\alpha_2}}} \sum_{q=1}^{N} h_q g_q \varphi_q x + n_2, \tag{4}$$

in which N represents the number of reflecting elements, P_s denotes the transmission power of the RS. The variables d_1 and d_2 are the distance between the RS and IRS, and between the IRS and the destination, respectively, with α_1 and α_2 denoting the path-loss exponents. Here, $\varphi_q = \zeta_q e^{j\theta_q}$ is the response of the IRS, where ζ_q and θ_q are the amplitude reflection coefficient and the phase shift induced by the IRS, respectively. Here, we assume that h_q, g_q, and their phases (θ_{h_q} and θ_{g_q}) are known and can be perfectly compensated at the IRS, i.e., $\theta_q = -(\theta_{h_q} + \theta_{g_q})$. The channel coefficients between the RS and IRS, i.e., h_q, and between the IRS and the destination, i.e., g_q, follows the Rice fading model, whose envelope PDF is given by [26]

$$f_{U_q}(u) = \frac{u}{\sigma_q^2} \exp\left(-\frac{u^2 + \nu_q^2}{2\sigma_q^2}\right) I_0\left(\frac{\nu_q}{\sigma_q^2} u\right). \tag{5}$$

Here, $U_q \in \{h_q, g_q\}$, ν_q^2 is the power of the LoS component, $2\sigma_q^2$ is the power of the multi-path components. Let $K_q = \frac{\nu_q^2}{2\sigma_q^2}$ represents the power ratio between the LoS and the mutli-path components.

The k-th moment of U_q, $\mathbb{E}\left[U^k\right]$, can be derived in a closed-form as [27, Eq. (3.15.2.9)]

$$\mathbb{E}\left[U_q^k\right] = \left(\sqrt{2}\sigma_q\right)^{\frac{k}{2}} \Gamma\left(\frac{k}{2} + 1\right) L_{\frac{k}{2}}^0\left(-\frac{\nu_q^2}{2\sigma_q^2}\right), \tag{6}$$

where $\Gamma(\cdot)$ denotes the Gamma function [25, Eq. (8.310)] and $L_k^0(\cdot)$ is k-th order Laguerre polynomial [25, Eq. (8.970)].

Capitalizing on (1) and (4), the received instantaneous SNRs γ_1 and γ_2 can be respectively expressed as

$$\gamma_1 = \overline{\gamma}_1 |h|^2 r^{-\alpha}, \tag{7}$$

and

$$\gamma_2 = \frac{\overline{\gamma}_2}{d_1^{\alpha_1} d_2^{\alpha_2}} H^2, \tag{8}$$

where $\overline{\gamma}_1 = \frac{P_t}{\sigma^2_{n_1}}$, $\overline{\gamma}_2 = \frac{P_s}{\sigma^2_{n_2}}$, and $H = \sum_{q=1}^{N} |h_p||g_p|$.

Proposition 1. *For independent and identically distributed h_q and g_q, $\forall q = 1, \ldots, N$, the PDF and the CDF of the instantaneous received SNR γ_1 can be respectively expressed as in* (9) *and* (10)*, where $\mathrm{G}_{\cdot,\cdot}^{-,-}[\cdot]$ is the Meijer's G-function* [28, Eq. (8.2.1.1)] *and $\Psi_\ell = \frac{1}{\alpha}(\beta_\ell + 1)$.*

$$f_{\gamma_1}(\gamma) = \frac{1}{\alpha} \exp\left(-\frac{m\lambda^2}{\Omega}\right) \sum_{\ell=1}^{n} \sum_{l=0}^{p} B_\ell\, C(l, p, m-1) \left(\frac{m\lambda^2}{\Omega}\right)^l \times \gamma^{-1} \mathrm{G}_{1,2}^{1,1}\left[\frac{mD^\alpha}{\Omega\overline{\gamma}_1}\gamma \,\middle|\, \begin{matrix} 1-\Psi_\ell \\ m+l, -\Psi_\ell \end{matrix}\right], \tag{9}$$

and

$$F_{\gamma_1}(\gamma) = \frac{1}{\alpha} \exp\left(-\frac{m\lambda^2}{\Omega}\right) \sum_{\ell=1}^{n} \sum_{l=0}^{p} B_\ell\, C(l, p, m-1) \times \left(\frac{m\lambda^2}{\Omega}\right)^l \mathrm{G}_{2,3}^{1,2}\left[\frac{mD^\alpha}{\Omega\overline{\gamma}_1}\gamma \,\middle|\, \begin{matrix} 1-\Psi_\ell, 1 \\ m+l, 0, -\Psi_\ell \end{matrix}\right]. \tag{10}$$

Proof: See Appendix A. ∎

Proposition 2. *The PDF and the CDF of the instantaneous received SNR γ_2 can be accurately expressed as in* (11) *and* (12)*, respectively,*

$$f_{\gamma_2}(\gamma) = \frac{a_1 a_2}{2\gamma} \mathrm{G}_{1,2}^{2,0}\left[\frac{\sqrt{d_1^{\alpha_1} d_2^{\alpha_2}}}{a_2\sqrt{\overline{\gamma}_2}}\sqrt{\gamma} \,\middle|\, \begin{matrix} a_3+1 \\ a_4+1, a_5+1 \end{matrix}\right], \tag{11}$$

TABLE I
THE VALUES OF ζ AND δ FOR DIFFERENT MODULATION SCHEMES

Modulation Scheme	ζ	δ
Coherent binary frequency-shift keying (CBFSK)	$\frac{1}{2}$	$\frac{1}{2}$
Coherent binary phase-shift keying (CBPSK)	$\frac{1}{2}$	1
Non-coherent binary frequency-shift keying (NBFSK)	1	$\frac{1}{2}$
Differential binary phase-shift keying (DBPSK)	1	1
M-ary pulse amplitude modulation (M-PAM)	$\frac{1}{2}$	$\delta = \log_2(M)/8(M-1)^2$

and

$$F_{\gamma_2}(\gamma) = a_1 a_2 \mathrm{G}_{2,3}^{2,1}\left[\frac{\sqrt{d_1^{\alpha_1} d_2^{\alpha_2}}}{a_2\sqrt{\overline{\gamma}_2}}\sqrt{\gamma}\,\middle|\, \begin{matrix} 1, a_3+1 \\ a_4+1, a_5+1, 0 \end{matrix}\right], \tag{12}$$

whereby

$$a_1 = \frac{\Gamma(a_3+1)}{a_2\Gamma(a_4+1)\Gamma(a_5+1)}, \tag{13}$$

$$a_3 = \frac{4\varphi_4 - 9\varphi_3 + 6\varphi_2 - \mu_1}{-\varphi_4 + 3\varphi_3 - 3\varphi_2 + \mu_1}, \tag{14}$$

$$a_2 = \frac{a_3}{2}(\varphi_4 - 2\varphi_3 + \varphi_2) + 2\varphi_4 - 3\varphi_3 + \varphi_2, \tag{15}$$

$$a_4 = \frac{a_6 + a_7}{2}, \tag{16}$$

$$a_5 = \frac{a_6 - a_7}{2}, \tag{17}$$

$$a_6 = \frac{a_3(\varphi_2 - \mu_1) + 2\varphi_2 - \mu_1}{a_2} - 3, \tag{18}$$

$$a_7 = \sqrt{(a_6+2)^2 - \frac{4\mu_1(a_3+1)}{a_2}}, \tag{19}$$

$$\varphi_k = \frac{\mu_k}{\mu_{k-1}}, \qquad k \geq 1. \tag{20}$$

The parameter μ_k denotes the k-th moment of the RV H.

Proof: See Appendix A. ∎

III. PERFORMANCE ANALYSIS

A. Outage Probability

The outage probability of the DaF dual-hop communication system under consideration can be obtained by finding the CDF of the end-to-end SNR. The end-to-end SNR γ_t can be written as $\gamma_t = \min\{\gamma_1, \gamma_2\}$. Therefore, the CDF of γ_t can be expressed as

$$F_{\gamma_t}(\gamma) = F_{\gamma_1}(\gamma) + F_{\gamma_2}(\gamma) - F_{\gamma_1}(\gamma)F_{\gamma_2}(\gamma), \tag{21}$$

whereby $F_{\gamma_i}(\gamma)$, $i = 1, 2$, denotes the CDF of γ_i.

The outage probability can be obtained by substituting (10) and (12) into (21), with $\gamma = \gamma_{\text{th}}$, whereby γ_{th} is a predefined threshold, and using the definition of the Meijer's G-function of two variables [29, Eq. (13.1)], the outage probability can be obtained as in (22), at the top of the next page, where $\mathrm{G}_{-,=:-,-:-,-}^{-,-:-,-:-,-}[\cdot]$ is the Meijer's G-function of two variables.

B. Average Bit Error rate

For various coherent and non-coherent modulation schemes, the average BER for the system under consideration can be expressed as

$$\overline{P}_b = \overline{P}_{b,1} + \overline{P}_{b,2} - 2\overline{P}_{b,1}\overline{P}_{b,2}, \tag{23}$$

where $\overline{P}_{b,1}$ and $\overline{P}_{b,2}$ are the average BERs of the first- and second-hop, respectively, which can be derived via

$$\overline{P}_{b,i} = \frac{\delta^\zeta}{2\Gamma(\zeta)}\int_0^\infty \gamma^{\zeta-1}\exp(-\delta\gamma)F_{\gamma_i}(\gamma)\,\mathrm{d}\gamma, \tag{24}$$

whereby $i = 1, 2$, δ and ζ are modulation-dependent parameters. The values of δ and ζ are summarized in Table I.

Substituting (10) and (12) into (24), results in

$$\overline{P}_{b,1} = \frac{\delta^\zeta \exp\left(-\frac{m\lambda^2}{\Omega}\right)}{2\alpha\Gamma(\zeta)}\sum_{\ell=1}^{n}\sum_{l=0}^{p} B_\ell\, C(l,p,m-1)\left(\frac{m\lambda^2}{\Omega}\right)^l \times \int_0^\infty \gamma^{\zeta-1}\exp(-\delta\gamma)\mathrm{G}_{2,3}^{1,2}\left[\frac{mD^\alpha}{\Omega\overline{\gamma}_1}\gamma\,\middle|\, \begin{matrix} 1-\Psi_\ell, 1 \\ m+l, 0, -\Psi_\ell \end{matrix}\right]\mathrm{d}\gamma, \tag{25}$$

and

$$\overline{P}_{b,2} = \frac{a_1 a_2 \delta^\zeta}{2\Gamma(\zeta)}\int_0^\infty \gamma^{\zeta-1}\exp(-\delta\gamma) \times \mathrm{G}_{2,3}^{2,1}\left[\frac{\sqrt{d_1^{\alpha_1} d_2^{\alpha_2}}}{a_2\sqrt{\overline{\gamma}_2}}\sqrt{\gamma}\,\middle|\, \begin{matrix} 1, a_3+1 \\ a_4+1, a_5+1, 0 \end{matrix}\right]\mathrm{d}\gamma, \tag{26}$$

The above two integrals can be solved in closed-form, with the aid of [28, Eq. (2.24.3.1)], as

$$\overline{P}_{b,1} = \frac{\exp\left(-\frac{m}{\Omega}\lambda^2\right)}{2\alpha\Gamma(\zeta)}\sum_{\ell=1}^{n}\sum_{l=0}^{p}\frac{B_\ell}{D^{\beta_\ell+1}}C(l,p,m-1)\left(\frac{m\lambda^2}{\Omega}\right)^l \times \left(\frac{\Omega\delta\overline{\gamma}_1}{m}\right)^{\Psi_\ell}\mathrm{G}_{3,3}^{1,3}\left[\frac{mD^\alpha}{\Omega\delta\overline{\gamma}_1}\,\middle|\, \begin{matrix} 1+\Psi_\ell-\zeta, 1, 1+\Psi_\ell \\ m+l+\Psi_\ell, \Psi_\ell, 0 \end{matrix}\right], \tag{27}$$

and

$$\overline{P}_{b,2} = \frac{a_1 a_2\, 2^{a_4+a_5-a_3-1}}{\sqrt{\pi}\Gamma(\zeta)} \times \mathrm{G}_{5,6}^{4,3}\left[\frac{d_1^{\alpha_1} d_2^{\alpha_2}}{4\delta a_2^2\overline{\gamma}_2}\,\middle|\, \begin{matrix} 1-\zeta, \frac{1}{2}, 1, \frac{a_3+1}{2}, \frac{a_3+2}{2} \\ \frac{a_4+1}{2}, \frac{a_4+2}{2}, \frac{a_5+1}{2}, \frac{a_5+2}{2}, 0, \frac{1}{2} \end{matrix}\right]. \tag{28}$$

$$P_{\text{out}} = a_1 a_2 \mathrm{G}_{2,3}^{2,1}\left[\frac{\sqrt{d_1^{\alpha_1} d_2^{\alpha_2}\gamma_{\text{th}}}}{a_2\sqrt{\overline{\gamma}_2}}\middle|\begin{matrix}1, a_3+1\\ a_4+1, a_5+1, 0\end{matrix}\right] + \frac{\exp\left(-\frac{m\lambda^2}{\Omega}\right)}{\alpha}\sum_{\ell=1}^{n}\sum_{l=0}^{p} B_\ell\, C(l,p,m-1)\left(\frac{m\lambda^2}{\Omega}\right)^l$$
$$\times\left\{\mathrm{G}_{2,3}^{1,2}\left[\frac{mD^\alpha\gamma_{\text{th}}}{\Omega\overline{\gamma}_1}\middle|\begin{matrix}1-\Psi_\ell, 1\\ m+l, 0, -\Psi_\ell\end{matrix}\right] - a_1 a_2 \mathrm{G}_{0,0:2,3:2,3}^{0,0:1,2:2,1}\left[\begin{matrix}-\\ -\end{matrix}\middle|\begin{matrix}1-\Psi_\ell, 1\\ m+l, 0, -\Psi_\ell\end{matrix}\middle|\begin{matrix}1, a_3+1\\ a_4+1, a_5+1, 0\end{matrix}\middle|\frac{mD^\alpha\gamma_{\text{th}}}{\Omega\overline{\gamma}_1}, \frac{\sqrt{d_1^{\alpha_1} d_2^{\alpha_2}\gamma_{\text{th}}}}{a_2\sqrt{\overline{\gamma}_2}}\right]\right\} \tag{22}$$

$$\overline{P}_b = \frac{a_1 a_2\, 2^{a_4+a_5-a_3-1}}{\sqrt{\pi}\Gamma(\zeta)}\mathrm{G}_{5,6}^{4,3}\left[\frac{d_1^{\alpha_1} d_2^{\alpha_2}}{4\delta a_2^2\overline{\gamma}_2}\middle|\begin{matrix}1-\zeta, \frac{1}{2}, 1, \frac{a_3+1}{2}, \frac{a_3+2}{2}\\ \frac{a_4+1}{2}, \frac{a_4+2}{2}, \frac{a_5+1}{2}, \frac{a_5+2}{2}, 0, \frac{1}{2}\end{matrix}\right] + \frac{\exp\left(-\frac{m}{\Omega}\lambda^2\right)}{2\alpha\Gamma(\zeta)}\sum_{\ell=1}^{n}\sum_{l=0}^{p}\frac{B_\ell}{D^{\beta_\ell+1}}C(l,p,m-1)\left(\frac{m\lambda^2}{\Omega}\right)^l$$
$$\times\left(\frac{\Omega\delta\overline{\gamma}_1}{m}\right)^{\Psi_\ell}\left\{\mathrm{G}_{3,3}^{1,3}\left[\frac{mD^\alpha}{\Omega\delta\overline{\gamma}_1}\middle|\begin{matrix}1+\Psi_\ell-\zeta, 1, 1+\Psi_\ell\\ m+l+\Psi_\ell, \Psi_\ell, 0\end{matrix}\right] - \frac{a_1 a_2\, 2^{a_4+a_5-a_3}}{\sqrt{\pi}\Gamma(\zeta)}\right.$$
$$\left.\times\,\mathrm{G}_{0,0:3,3:5,6}^{0,0:1,3:4,3}\left[\begin{matrix}-\\ -\end{matrix}\middle|\begin{matrix}1+\Psi_\ell-\zeta, 1, 1+\Psi_\ell\\ m+l+\Psi_\ell, \Psi_\ell, 0\end{matrix}\middle|\begin{matrix}1-\zeta, \frac{1}{2}, 1, \frac{a_3+1}{2}, \frac{a_3+2}{2}\\ \frac{a_4+1}{2}, \frac{a_4+2}{2}, \frac{a_5+1}{2}, \frac{a_5+2}{2}, 0, \frac{1}{2}\end{matrix}\middle|\frac{mD^\alpha}{\Omega\delta\overline{\gamma}_1}, \frac{d_1^{\alpha_1} d_2^{\alpha_2}}{4\delta a_2^2\overline{\gamma}_2}\right]\right\} \tag{29}$$

Substituting (27) and (28) into (23), the average BER for the DaF system under consideration can be obtained in closed-form as in (29).

C. Ergodic Channel Capacity

The ergodic channel capacity for the dual-hop DaF system under consideration can be can be evaluated using the following formula

$$\overline{\mathtt{CAP}} = \frac{1}{2}\min\left\{\overline{\mathtt{CAP}}_1, \overline{\mathtt{CAP}}_2\right\}, \tag{30}$$

whereby $\overline{\mathtt{CAP}}_i$, $i = 1, 2$, represents the ergodic channel capacity of the i^{th}-hop, which is defined as $\overline{\mathtt{CAP}}_i \triangleq \mathbb{E}\big[\log_2(1+\gamma_i)\big]$. As such, the ergodic channel capacity, for the i^{th}-hop, can be derived using

$$\overline{\mathtt{CAP}}_i = \frac{1}{\ln(2)}\int_0^\infty \ln(1+\gamma_i) f_{\gamma_i}(\gamma)\mathrm{d}\gamma \qquad \text{[b/s/Hz]}. \tag{31}$$

Representing the logarithmic function in (31) in terms of Meijer's G-function [28, Eq. (3.4.6.5)], using (9) and (11). The capacity for the first- and second-hop can be respectively expressed as in (32) and (33). With the help of [28, Eq. (2.24.1.1)], using (32), and (33), the ergodic channel capacity for the first- and second-hop can be respectively derived in closed-forms as

$$\overline{\mathtt{CAP}}_1 = \frac{\exp\left(-\frac{m\lambda^2}{\Omega}\right)}{\alpha\ln(2)}\sum_{\ell=1}^{n}\sum_{l=0}^{p} B_\ell\, C(l,p,m-1)\left(\frac{m\lambda^2}{\Omega}\right)^l$$
$$\times\,\mathrm{G}_{3,4}^{3,2}\left[\frac{mD^\alpha}{\Omega\overline{\gamma}_1}\middle|\begin{matrix}1-\Psi_\ell, 0, 1\\ m+l, 0, 0, -\Psi_\ell\end{matrix}\right], \tag{34}$$

and

$$\overline{\mathtt{CAP}}_2 = \frac{a_1 a_2 2^{a_4+a_5-a_3}}{\sqrt{\pi}\ln(2)}$$
$$\times\,\mathrm{G}_{4,6}^{6,1}\left[\frac{d_1^{\alpha_1} d_2^{\alpha_2}}{4a_2^2\overline{\gamma}_2}\middle|\begin{matrix}0, 1, \frac{a_3+1}{2}, \frac{a_3+2}{2}\\ \frac{a_4+1}{2}, \frac{a_4+2}{2}, \frac{a_5+1}{2}, \frac{a_5+2}{2}, 0, 0\end{matrix}\right]. \tag{35}$$

Finally, the ergodic channel capacity for the system under consideration can be obtained after substituting (34) and (35) into (30). The result is shown in (36), at the top of the next page.

IV. Asymptotic Analysis

To gain more insight into the derived performance metrics derived in Sec. III, in this section, simple and accurate asymptotic analytical expressions in the high SNR regime are derived. To this end, the PDFs of γ_1 and γ_2 should be approximated around the origin [30]. As such, by sequentially applying the relationship between the Meijer's G-function and the Fox's H-function [28, Eq. (8.3.2.21)] and then using [31, Theorem 1.11], the PDFs of γ_1 and γ_2 can be respectively approximated as

$$f_{\gamma_1}(\gamma) \approx \frac{\exp\left(-\frac{m\lambda^2}{\Omega}\right)}{\alpha}\sum_{\ell=1}^{n}\sum_{l=0}^{p} B_\ell\, C(l,p,m-1)\lambda^{2l}\left(\frac{m}{\Omega}\right)^{m+2l}$$
$$\times\,\frac{\gamma^{m+l-1}}{(m+l+\Psi_\ell)\left(\overline{\gamma}_1 D^{-\alpha}\right)^{m+l}}, \tag{37}$$

and

$$f_{\gamma_2}(\gamma) \approx \frac{a_1 a_2\Gamma(a_7)}{2\Gamma(a_3-a_5)\gamma}\left(\frac{\sqrt{d_1^{\alpha_1} d_2^{\alpha_2}}}{a_2\sqrt{\overline{\gamma}_2}}\sqrt{\gamma}\right)^{a_5+1} \tag{38}$$

A. Asymptotic Outage Probability

At high SNR values, the asymptotic outage probability expression can be expressed as

$$F_{\gamma_t}^{\infty}(\gamma) = F_{\gamma_1}^{\infty}(\gamma) + F_{\gamma_2}^{\infty}(\gamma) - F_{\gamma_1}^{\infty}(\gamma)F_{\gamma_2}^{\infty}(\gamma)$$
$$\approx F_{\gamma_1}^{\infty}(\gamma) + F_{\gamma_2}^{\infty}(\gamma), \tag{39}$$

where $F_{\gamma_i}^{\infty}(\cdot)$ is the asymptotic outage probability as $\overline{\gamma}_i \to \infty$. For the two hops, the asymptotic outage probability can be respectively obtained with the help of (37) and (38) as

$$F_{\gamma_1}(\gamma_{\text{th}}) \approx \frac{\exp\left(-\frac{m\lambda^2}{\Omega}\right)}{\alpha}\sum_{\ell=1}^{n}\sum_{l=0}^{p} B_\ell\, C(l,p,m-1)\left(\frac{\lambda^2 m}{\Omega}\right)^l$$
$$\times\,\frac{(m\gamma_{\text{th}})^{m+l}}{(m+l)(m+l+\Psi_\ell)\left(\Omega\overline{\gamma}_1 D^{-\alpha}\right)^{m+l}}, \tag{40}$$

$$\overline{\mathrm{CAP}}_1 = \frac{\exp\left(-\frac{m\lambda^2}{\Omega}\right)}{\alpha\ln(2)}\sum_{\ell=1}^{n}\sum_{l=0}^{p} B_\ell\, C(l,p,m-1)\left(\frac{m\lambda^2}{\Omega}\right)^{l}\int_0^\infty \gamma^{-1}\mathrm{G}_{2,2}^{1,2}\left[\gamma\left|\begin{matrix}1,1\\1,0\end{matrix}\right.\right]\mathrm{G}_{1,2}^{1,1}\left[\frac{mD^\alpha}{\Omega\overline{\gamma}_1}\gamma\left|\begin{matrix}1-\Psi_\ell\\ m+l,-\Psi_\ell\end{matrix}\right.\right]\mathrm{d}\gamma \tag{32}$$

$$\overline{\mathrm{CAP}}_2 = \frac{a_1 a_2}{2\ln(2)}\int_0^\infty \gamma^{-1}\mathrm{G}_{2,2}^{1,2}\left[\gamma\left|\begin{matrix}1,1\\1,0\end{matrix}\right.\right]\mathrm{G}_{1,2}^{2,0}\left[\frac{\sqrt{d_1^{\alpha_1}d_2^{\alpha_2}}}{a_2\sqrt{\overline{\gamma}_2}}\sqrt{\gamma}\left|\begin{matrix}a_3+1\\ a_4+1, a_5+1\end{matrix}\right.\right]\mathrm{d}\gamma \tag{33}$$

$$\overline{\mathrm{CAP}} = \frac{1}{2}\min\left\{\frac{\exp\left(-\frac{m\lambda^2}{\Omega}\right)}{\alpha\ln(2)}\sum_{\ell=1}^{n}\sum_{l=0}^{p} B_\ell\, C(l,p,m-1)\left(\frac{m\lambda^2}{\Omega}\right)^{l}\mathrm{G}_{3,4}^{3,2}\left[\frac{mD^\alpha}{\Omega\overline{\gamma}_1}\left|\begin{matrix}1-\Psi_\ell,0,1\\ m+l,0,0,-\Psi_\ell\end{matrix}\right.\right],\right.$$
$$\left.\frac{a_1 a_2 2^{a_4+a_5-a_3}}{\sqrt{\pi}\ln(2)}\mathrm{G}_{4,6}^{6,1}\left[\frac{d_1^{\alpha_1}d_2^{\alpha_2}}{4a_2^2\overline{\gamma}_2}\left|\begin{matrix}0,1,\frac{a_3+1}{2},\frac{a_3+2}{2}\\ \frac{a_4+1}{2},\frac{a_4+2}{2},\frac{a_5+1}{2},\frac{a_5+2}{2},0,0\end{matrix}\right.\right]\right\} \tag{36}$$

and

$$F_{\gamma_2}(\gamma) \approx \frac{a_1 a_2\Gamma(a_7)}{(a_5+1)\Gamma(a_3-a_5)}\left(\frac{\sqrt{d_1^{\alpha_1}d_2^{\alpha_2}}}{a_2\sqrt{\overline{\gamma}_2}}\sqrt{\gamma_{\text{th}}}\right)^{a_5+1}. \tag{41}$$

Substituting (40) and (41) into (39), then the asymptotic outage probability can be expressed as in (42), at the top of the next page. Note that in the high SNR regime, the outage probability can be given as $P_{out}^{\infty} \propto \overline{\gamma}^{-G_d}$, whereby G_d represents the diversity gain. Thus, it is clear from (40) that the diversity gain of the first-hop is $G_d = m$. However, for the second-hop the diversity gain is a function of the parameter a_5. In the simulation results, we show that the diversity order is related to the number of reflecting elements N, while the LoS component K provides no diversity advantage. Therefore, the diversity gain of the DaF system is $G_d = \min(N, m)$.

B. Asymptotic Average Bit Error Rate

In the high SNR regime, the asymptotic average BER for the system under consideration can be written as

$$\begin{aligned}\overline{P}_b^{\infty} &= \overline{P}_{b,1}^{\infty} + \overline{P}_{b,2}^{\infty} - 2\overline{P}_{b,1}^{\infty}\overline{P}_{b,2}^{\infty}\\ &\approx \overline{P}_{b,1}^{\infty} + \overline{P}_{b,2}^{\infty},\end{aligned} \tag{43}$$

where

$$\overline{P}_{b,i}^{\infty} \approx \frac{\delta^\zeta}{2\Gamma(\zeta)}\int_0^\infty \gamma^{\zeta-1}\exp(-\delta\gamma)F_{\gamma_i}^{\infty}(\gamma)\,\mathrm{d}\gamma. \tag{44}$$

Replacing γ_{th} with γ in (40) and (41), using (44) and [25, Eq. (3.381.4)], the asymptotic average BER for the first- and second-hop can be respectively obtained as

$$\overline{P}_{b,1}^{\infty} \approx \frac{\exp\left(-\frac{m\lambda^2}{\Omega}\right)}{2\alpha\Gamma(\zeta)}\sum_{\ell=1}^{n}\sum_{l=0}^{p} B_\ell\, C(l,p,m-1)\lambda^{2l}\left(\frac{m}{\Omega}\right)^{m+2l} \times \frac{\Gamma(\zeta+m+l)}{(m+l)(m+l+\Psi_\ell)(\delta\overline{\gamma}_1 D^{-\alpha})^{m+l}}. \tag{45}$$

and

$$\overline{P}_{b,2}^{\infty} = \frac{a_1 a_2\Gamma(a_7)\Gamma\left(\zeta+\frac{a_5+1}{2}\right)}{2(a_5+1)\Gamma(\zeta)\Gamma(a_3-a_5)}\left(\frac{d_1^{\alpha_1}d_2^{\alpha_2}}{\delta a_2^2\overline{\gamma}_2}\right)^{\frac{a_5+1}{2}}. \tag{46}$$

Substituting (45) and (46), the asymptotic average BER, in the high SNR regime, can be expressed as in (47), at the top of the next page. Similar, to the outage probability, the diversity gain can be given as $G_d = \min(N, m)$.

C. Asymptotic Ergodic Channel Capacity

In the high SNR regime, the ergodic channel capacity can be simply and accurately approximated by

$$\overline{\mathrm{CAP}}_i^{\infty} \approx \log_2(\overline{\gamma}_i) + \log_2(e)\frac{\partial}{\partial k}\left.\frac{\mathbb{E}[\gamma_i^k]}{\overline{\gamma}_i^k}\right|_{k=0}, \tag{48}$$

whereby $\frac{\partial}{\partial k}$ denote the first derivative operator and $\mathbb{E}[\cdot]$ is the expectation operator. Using (9), (11), and with the help of [28, Eq. (2.24.2.1)], the k-th moment of each hop can be respectively obtained as

$$\mathbb{E}[\gamma_1^k] = \frac{1}{\alpha}\exp\left(-\frac{m\lambda^2}{\Omega}\right)\sum_{\ell=1}^{n}\sum_{l=0}^{p} B_\ell\, C(l,p,m-1)\left(\frac{m\lambda^2}{\Omega}\right)^{l} \times \left(\frac{\Omega\overline{\gamma}_1}{mD^\alpha}\right)^{k}\frac{\Gamma(m+l+k)\Gamma(\Psi_\ell-k)}{\Gamma(1+\Psi_\ell-k)}, \tag{49}$$

and

$$\mathbb{E}[\gamma_2^k] = a_1 a_2\left(\frac{a_2^2\overline{\gamma}_2}{d_1^{\alpha_1}d_2^{\alpha_2}}\right)^{k}\frac{\Gamma(a_4+2k+1)\Gamma(a_5+2k+1)}{\Gamma(a_3+2k+1)} \tag{50}$$

Capitalizing on (48), (49), and (50) the asymptotic ergodic channel capacity, in the high SNR regime, for the first- and second-hop can be respectively obtained as

$$\begin{aligned}\overline{\mathrm{CAP}}_1^{\infty} &\approx \log_2(\overline{\gamma}_1) + \frac{\log_2(e)}{\alpha}\exp\left(-\frac{m\lambda^2}{\Omega}\right)\sum_{\ell=1}^{n}\sum_{l=0}^{p} B_\ell\\ &\times C(l,p,m-1)\left(\frac{m\lambda^2}{\Omega}\right)^{l}\frac{\Gamma(m+l)\Gamma(\Psi_\ell)}{\Gamma(1+\Psi_\ell)}\\ &\times\left\{\ln\left(\frac{\Omega}{mD^\alpha}\right)\psi(m+l) + \psi\big(1+\Psi_\ell\big) - \psi\big(\Psi_\ell\big)\right\}\end{aligned} \tag{51}$$

$$F_{\gamma_t}^{\infty}(\gamma) \approx \frac{\exp\left(-\frac{m\lambda^2}{\Omega}\right)}{\alpha} \sum_{\ell=1}^{n} \sum_{l=0}^{p} B_\ell\, C(l,p,m-1) \left(\frac{\lambda^2 m}{\Omega}\right)^{l} \frac{(m\gamma_{\text{th}})^{m+l}}{(m+l)\,(m+l+\Psi_\ell)\,(\Omega\overline{\gamma}_1 D^{-\alpha})^{m+l}} + \frac{a_1 a_2 \Gamma(a_7)}{(a_5+1)\Gamma(a_3-a_5)} \left(\frac{\sqrt{d_1^{\alpha_1} d_2^{\alpha_2}}}{a_2\sqrt{\overline{\gamma}_2}} \sqrt{\gamma_{\text{th}}}\right)^{a_5+1} \tag{42}$$

$$\overline{P}_b^{\infty} \approx \frac{\exp\left(-\frac{m\lambda^2}{\Omega}\right)}{2\alpha\Gamma(\zeta)} \sum_{\ell=1}^{n} \sum_{l=0}^{p} B_\ell\, C(l,p,m-1) \lambda^{2l} \left(\frac{m}{\Omega}\right)^{m+2l} \frac{\Gamma(\zeta+m+l)}{(m+l)\,(m+l+\Psi_\ell)\,(\delta\overline{\gamma}_1 D^{-\alpha})^{m+l}} + \frac{a_1 a_2 \Gamma(a_7)\Gamma\left(\zeta+\frac{a_5+1}{2}\right)}{2(a_5+1)\Gamma(\zeta)\Gamma(a_3-a_5)} \left(\frac{d_1^{\alpha_1} d_2^{\alpha_2}}{\delta a_2^2 \overline{\gamma}_2}\right)^{\frac{a_5+1}{2}} \tag{47}$$

and

$$\overline{\text{CAP}}_2^{\infty} \approx \log_2(\overline{\gamma}_2) + \frac{a_1 a_2 \log_2(e)\Gamma(a_4+1)\Gamma(a_5+1)}{\Gamma(a_3+1)} \times \left\{ \ln\left(\frac{a_2^2}{d_1^{\alpha_1} d_2^{\alpha_2}}\right) + 2\psi(a_4+1) + 2\psi(a_5+1) - 2\psi(a_3+1) \right\} \tag{52}$$

whereby $\psi(\cdot)$ is the digamma function [25, Eq. (8.36)]. Thus, the asymptotic ergodic capacity in the high SNR regime can be written as in (53), at the top of the next page.

In the low SNR regime, the ergodic channel capacity can be approximated a

$$\overline{\text{CAP}}_i \approx \mathbb{E}[\gamma_i^k]\big|_{k=1}. \tag{54}$$

Based on (49), (50), and (54), the ergodic channel capacity at high SNR values for the first- and second-hop can be respectively expressed as

$$\overline{\text{CAP}}_1 \approx \frac{1}{\alpha} \exp\left(-\frac{m\lambda^2}{\Omega}\right) \sum_{\ell=1}^{n} \sum_{l=0}^{p} B_\ell\, C(l,p,m-1) \left(\frac{m\lambda^2}{\Omega}\right)^{l} \times \frac{\Omega\overline{\gamma}_1 \Gamma(m+l+1)\Gamma(\Psi_\ell-1)\log_2(e)}{m D^{\alpha}\Gamma(\Psi_\ell)}, \tag{55}$$

and

$$\overline{\text{CAP}}_2 \approx \frac{a_1 a_2^3 \overline{\gamma}_2 \Gamma(a_4+3)\Gamma(a_5+3)\log_2(e)}{d_1^{\alpha_1} d_2^{\alpha_2}\Gamma(a_3+3)}. \tag{56}$$

Thus, the asymptotic ergodic capacity in the low SNR regime can be written as in (57), at the top of the next page.

V. Numerical and Simulation Results

In this section, we present some numerical and Monte-Carlo simulation results to investigate the effect of system and channel parameters on the performance of outage probability, average BER for coherent BPSK modulation scheme, and ergodic channel capacity. Without loss of generality, the path-loss exponents, α, α_1, and α_2 are set to 2.5, $\Omega = 1$, the maximum radius $D = 50\,\text{m}$, the RS-to-IRS and IRS-to-GCS distances are set to $d_1 = d_2 = 15\,\text{m}$.

In Fig. 2 and Fig. 3, the outage performance of the second-hop is shown for different values of K and N, respectively. It

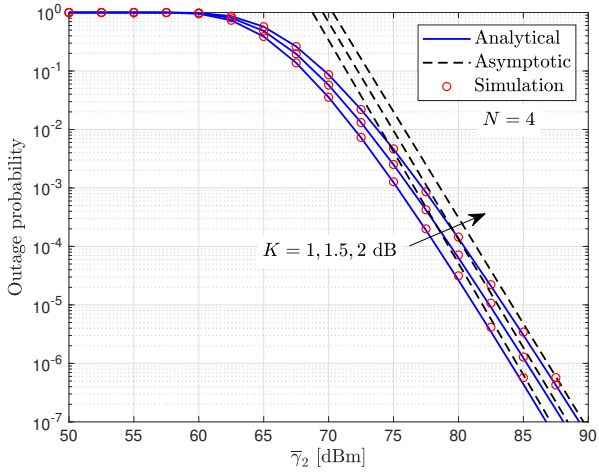

Fig. 2. Outage probability versus $\overline{\gamma}_2$ with $\gamma_{\text{th}} = 0$ dB.

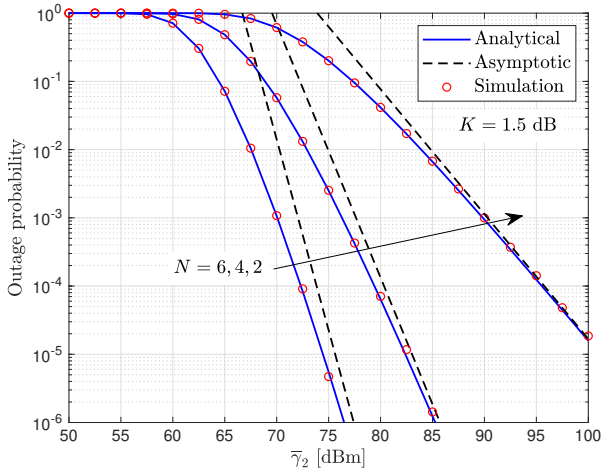

Fig. 3. Outage probability versus $\overline{\gamma}_2$ with $\gamma_{\text{th}} = 0$ dB.

is clear from Fig. 2 that the diversity gain is independent of the LoS component K, whereas the results in Fig. 3 show that the diversity gain depends on N, which confirms our conclusion in (41). In Fig. 4, the outage probability performance as a

$$\overline{\mathrm{CAP}}_{\mathrm{H}}^{\infty} \approx \frac{1}{2}\min\left\{\log_2(\overline{\gamma}_1) + \frac{\log_2(e)}{\alpha}\exp\left(-\frac{m\lambda^2}{\Omega}\right)\sum_{\ell=1}^{n}\sum_{l=0}^{p} B_\ell C(l,p,m-1)\left(\frac{m\lambda^2}{\Omega}\right)^l \frac{\Gamma(m+l)\Gamma(\Psi_\ell)}{\Gamma(1+\Psi_\ell)}\right.$$
$$\times\left\{\ln\left(\frac{\Omega}{mD^\alpha}\right)\psi(m+l)+\psi(1+\Psi_\ell)-\psi(\Psi_\ell)\right\}, \log_2(\overline{\gamma}_2) + \frac{a_1 a_2 \log_2(e)\Gamma(a_4+1)\Gamma(a_5+1)}{\Gamma(a_3+1)}$$
$$\left.\times\left\{\ln\left(\frac{a_2^2}{d_1^{\alpha_1} d_2^{\alpha_2}}\right)+2\psi(a_4+1)+2\psi(a_5+1)-2\psi(a_3+1)\right\}\right\} \quad (53)$$

$$\overline{\mathrm{CAP}}_{\mathrm{L}} \approx \frac{1}{2}\min\left\{\frac{1}{\alpha}\exp\left(-\frac{m\lambda^2}{\Omega}\right)\sum_{\ell=1}^{n}\sum_{l=0}^{p} B_\ell\, C(l,p,m-1)\left(\frac{m\lambda^2}{\Omega}\right)^l \frac{\Omega\overline{\gamma}_1\Gamma(m+l+1)\Gamma(\Psi_\ell-1)\log_2(e)}{mD^\alpha\Gamma(\Psi_\ell)},\right.$$
$$\left.\frac{a_1 a_2^3\,\overline{\gamma}_2\Gamma(a_4+3)\Gamma(a_5+3)\log_2(e)}{d_1^{\alpha_1} d_2^{\alpha_2}\Gamma(a_3+3)}\right\} \quad (57)$$

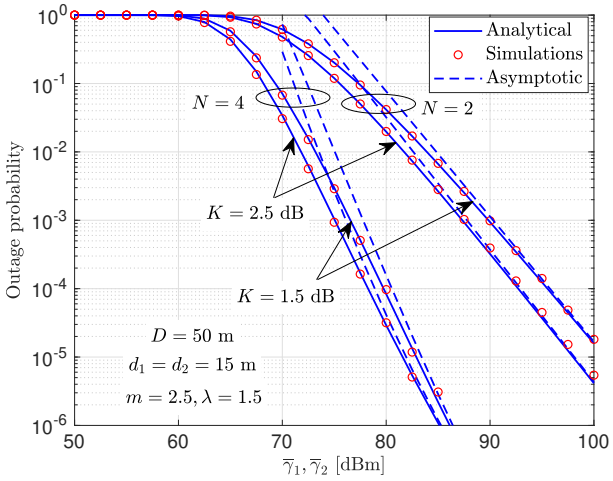

Fig. 4. Outage probability versus $\overline{\gamma}_1$ and $\overline{\gamma}_2$ with $\gamma_{\mathrm{th}} = 0$ dB.

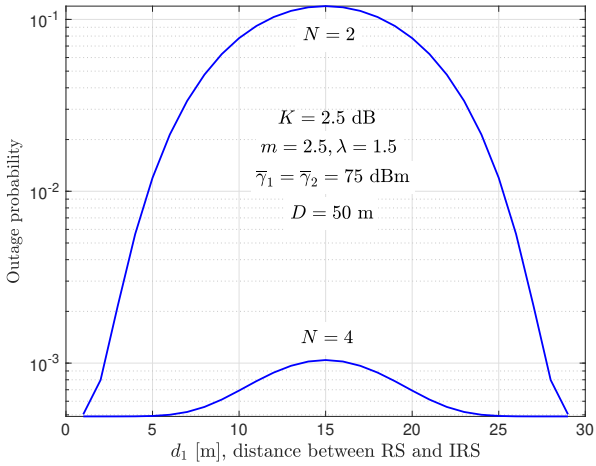

Fig. 5. Outage probability versus d_1 for $N = 2, 4$ and $\gamma_{\mathrm{th}} = 0$ dB.

function of $\overline{\gamma}_1$ and $\overline{\gamma}_2$ for different values of the number of reflecting elements N and the LoS component K. The threshold SNR $\gamma_{\mathrm{th}} = 0$ dB, $m = 2.5$, and $\lambda = 1.5$. The results show that the outage performance improves as the LoS component K and(or) the number of reflecting elements N increase(s). However, the effect of increasing N on the system performance is more pronounced than that of K. For example, to achieve an outage performance of 10^{-3}, when $N = 2$, the required SNRs for $K = 1.5, \text{and } 2.5$ dB are approximately 90 dBm and 87.5 dBm, respectively (i.e., with difference of 2.5 dBm). However, $K = 1.5$ dB, the required SNRs for $N = 2$ and 4 are approximately 90 dBm and 76 dBm, respectively (i.e., with difference of 14 dBm). In addition, the results show that the asymptotic curves match the analytical results at high SNR values.

The performance of the outage probability as a function of d_1, the RS-IRS distance, is shown in Fig. 5 for different values of N (i.e., $N = 2$ and $N = 4$). The other parameters are set as follows: $K = 1.5$ dB, $m = 2.5$, $\lambda = 1.5$, $\overline{\gamma}_1 = \overline{\gamma}_2 = 75$ dBm, and $\gamma_{\mathrm{th}} = 0$ dB. It can be seen that the outage probability is maximum when the IRS is located at a middle point between the RS and the GCS. However, a better performance can be achieved when the IRS is located either close to the RS or close to the destination.

The average BER performance of BPSK under different values λ (the LoS component between the UAV and the RS) and for $N = 2, 4$, $K = 1.5$ dB, and $m = 2.5$ is illustrated in Fig. 6. It can be seen that when the number of reflected elements $N = 2$, increasing λ has no effect on the BER performance. However, as N increase from 2 to 4, the system performance improves as λ increases. Also, the asymptotic curves follows the analytical ones at high SNR values. Not that the diversity gain $G_d = 2, 2.5$ when $N = 2, 4$, respectively, since $G_d = \min(N, m)$.

In Fig. 7, we show the results of the average BER for BPSK under different values of m, i.e., $m = 1, 1.5, 2.5, 3.5, 4.5, 5.5$, with $\lambda = 1$, $K = 1.5$ dB, and $N = 4$. The results show that the value of m has a noticeable impact on the system performance. However, when m becomes larger this impact becomes insignificant. Additionally, it can be seen that the diversity gain improves as m increases. However, as long as the values of m is less than N, the diversity gain G_d increase since

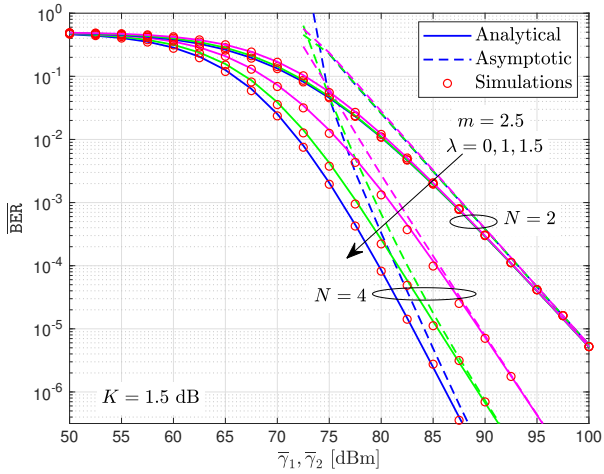

Fig. 6. BER performance of BPSK under different values of λ.

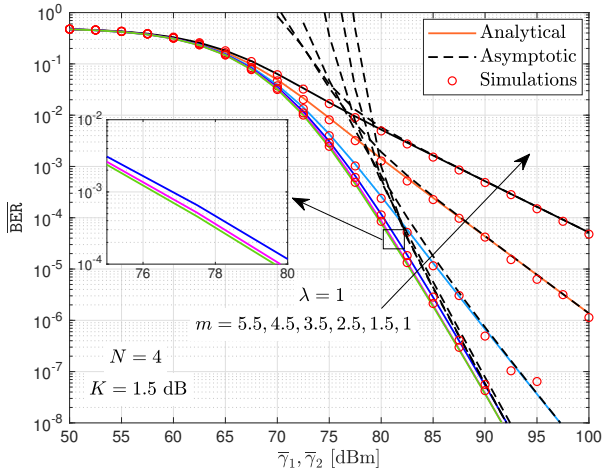

Fig. 7. BER performance for BPSK under different values of m.

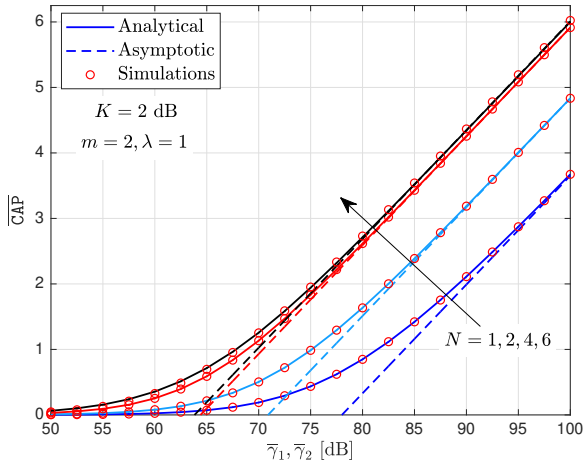

Fig. 8. Ergodic channel capacity performance under different values of N in the high SNR regime.

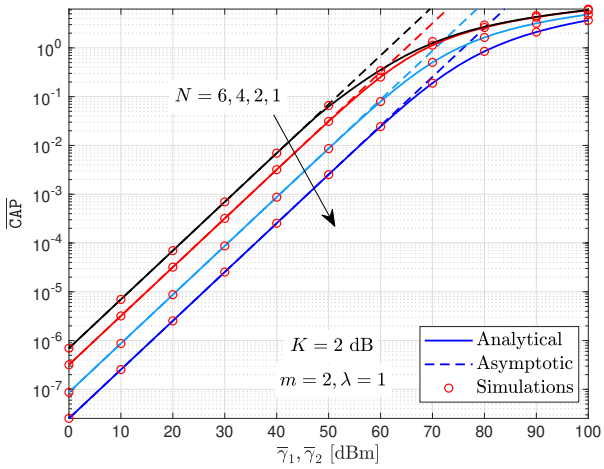

Fig. 9. Ergodic channel capacity performance under different values of N in the low SNR regime.

$G_d = \min(N, m)$. For example, when $m = 3.5, 4.5, 5.5$, the diversity gain $G_d = 3.5$. Whereas, when $m = 1, 1.5, 2.5, 3.5$, the diversity gain $G_d = 1, 1.5, 2.5, 3.5$, respectively. The performance of ergodic channel capacity is depicted in Fig. 8 and Fig. 9 for $N = 1, 2, 4, 6$, $K = 1.5$ dB, $\lambda = 1$, and $m = 2$. The results demonstrate that the capacity performance improves as the number of reflecting elements N increases. However, we have noticed that after a certain number of reflecting elements, in Fig. 8, increasing N larger than 6 has no effects on the system performance. This because the system capacity is limited by the minimum capacity between the two hops. Also, Fig. 8 shows that the asymptotic curves matches the analytical curves in the high SNR regime, which confirms our analysis. Note that Fig. 9 is provided here to validate the asymptotic capacity in the low SNR regime. It can be seen that the asymptotic curves matches the analytical ones, which verifies our analysis.

VI. Conclusions

In this paper, we have analyzed the performance of an IRS-aided DaF wireless system supporting the communication of a low altitude UAV with a GCS. We derived closed-form analytical expressions for the outage probability, average BER, and ergodic channel capacity. In addition, in the high SNR regime, accurate and simple expressions for the derived performance metrics were obtained. The results demonstrated that the system performance improves as the value of m, λ, K, and N increases. However, we have noticed that increasing one parameter at a time (e.g., m, λ, K or N), while other parameters stay fixed, improves the system performance as long as the value of this parameter is less than a certain value. Once the parameter reaches the threshold value, the improvement in the system performance becomes insignificant. Also, the results have demonstrated that the diversity gain G_d is limited by the number of reflecting elements N or the number of the multi-path components m, i.e., $\min(N, m)$.

APPENDIX A

Proof of Proposition 1

To find the PDF of γ_1, we first need to find the PDF of the RV $Z = |h|^2 r^{-\alpha}$. As such, let $W = |h|^2$ and $Y = r^{-\alpha}$. The PDF of W and Y can be found using the transformation of RV. Thus,

$$f_W(w) = \frac{A}{2} w^{\frac{1}{2}(m-1)} \exp\left(-\frac{m}{\Omega} w\right) I_{m-1}\left(\frac{2m\lambda}{\Omega}\sqrt{w}\right), \tag{58}$$

and

$$f_Y(y) = \frac{1}{\alpha} \sum_{\ell=1}^{n} \frac{B_\ell}{D^{\beta_\ell+1}} y^{-\frac{1}{\alpha}(\beta_\ell+1)-1}, \quad D^{-\alpha} \leq y \leq \infty. \tag{59}$$

The PDF of Z can be found using

$$f_Z(z) = \int_{D^{-\alpha}}^{\infty} \frac{1}{y} f_W\left(\frac{z}{y}\right) f_Y(y) \mathrm{d}y. \tag{60}$$

Substituting (58) and (59) into (60) yields (61). The Bessel function $I_\nu(\cdot)$ can be accurately approximated as

$$I_\nu(x) \simeq \sum_{l=0}^{p} C(l, n, \nu) \left(\frac{x}{2}\right)^{\nu+2l}, \tag{62}$$

where $C(l, p, \nu) = \frac{\Gamma(p+l)p^{1-2l}}{\Gamma(l+1)\Gamma(p-l+1)\Gamma(v+l+1)}$ [32]. Note that as $p \to \infty$, (62) reduces to the infinite series [25, Eq. (8.445)]. Now, using (62) and making change of variable $u = y^{-1}$, (61) can be rewritten as in (63). Using [25, Eq. (3.381.1)], the PDF of Z can be derived as in (64). Using (64), [28, Eq. (8.4.16.1)], [28, Eq. (8.2.2.15)], and after performing transformation of RVs using (7), the PDF of γ_1 can be obtained as in (9), whereas, the CDF in (10) can be obtained using [28, Eq. (2.24.2.2)]. Hence, the proof is completed.

Proof of Proposition 2

In light of the analysis in [33], the PDF of H can be accurately approximated in closed-form as

$$f_H(z) \approx a_1 G_{1,2}^{2,0}\left[\frac{z}{a_2}\middle|\begin{matrix} a_3 \\ a_4, a_5 \end{matrix}\right], \qquad z \geq 0. \tag{65}$$

Using (8), (65), and after performing transformation of RVs, the PDF of γ_2 can be obtained as in (11). Subsequently, the CDF in (12) can be obtained with the help of [28, Eq. (2.24.2.2)]. Thus, the proof is completed.

REFERENCES

[1] MarketsandMarkets. Unmanned Aerial Vehicle (UAV) market by vertical, class, system, industry (defense & security, agriculture, construction & mining, media & entertainment), type, mode of operation, range, point of sale, MTOW and region - global forecast to 2025. [Online]. Available: https://www.marketsandmarkets.com/Market-Reports/unmanned-aerial-vehicles-uav-market-662.html

[2] U. S. U. S. M. C. Command and S. College, *Unmanned aerial vehicles: Improving warfighting capabilities in the urban environment*. CreateSpace, 2014.

[3] D. Pinchera, Z. Qiu, X. Chu, C. Calvo-Ramirez, C. Briso, and X. Yin, "Low altitude UAV air-to-ground channel measurement and modeling in semiurban environments," *Wireless Communications and Mobile Computing*, vol. 2017, p. 1587412, 2017. [Online]. Available: https://doi.org/10.1155/2017/1587412

[4] J. Q. Cui et al., "Search and rescue using multiple drones in post-disaster situation," *Unmanned Systems*, vol. 04, no. 01, pp. 83–96, 2016. [Online]. Available: https://doi.org/10.1142/S2301385016400094

[5] H. Surmann, R. Worst, T. Buschmann, A. Leinweber, A. Schmitz, G. Senkowski, and N. Goddemeier, "Integration of uavs in urban search and rescue missions," in *2019 IEEE International Symposium on Safety, Security, and Rescue Robotics (SSRR)*, Sep. 2019, pp. 203–209.

[6] PRNewswire. Consumer drone market analysis - new opportunities explored, expansion at high cagr anticipated by 2024: Million insights. [Online]. Available: https://www.prnewswire.com/news-releases/consumer-drone-market-analysis—new-opportunities-explored-expansion-at-high-cagr-anticipated-by-2024-million-insights-301049078.html

[7] Y. Zeng, Q. Wu, and R. Zhang, "Accessing from the sky: A tutorial on uav communications for 5g and beyond," *Proceedings of the IEEE*, vol. 107, no. 12, pp. 2327–2375, Dec 2019.

[8] S. Li, B. Duo, X. Yuan, Y. Liang, and M. Di Renzo, "Reconfigurable intelligent surface assisted UAV communication: Joint trajectory design and passive beamforming," *IEEE Wireless Communications Letters*, vol. 9, no. 5, pp. 716–720, May 2020.

[9] D. Ma, M. Ding, and M. Hassan, "Enhancing cellular communications for uavs via intelligent reflective surface," in *2020 IEEE Wireless Communications and Networking Conference (WCNC)*, May 2020, pp. 1–6.

[10] G. Levin and S. Loyka, "Amplify-and-forward versus decode-and-forward relaying: Which is better?" in *22th International Zurich seminar on communications (IZS)*. Eidgenössische Technische Hochschule Zürich, 2012.

[11] L. Yang, Y. Yang, M. O. Hasna, and M. S. Alouini, "Coverage, probability of SNR gain, and DOR analysis of RIS-aided communication systems," *IEEE Wireless Communications Letters*, vol. 9, no. 8, pp. 1268–1272, Aug 2020.

[12] C. You, Z. Kang, Y. Zeng, and R. Zhang, "Enabling smart reflection in integrated air-ground wireless network: IRS meets UAV," *arXiv:2103.07151*, 2021.

[13] H. Hashida, Y. Kawamoto, and N. Kato, "Intelligent reflecting surface placement optimization in air-ground communication networks toward 6G," *IEEE Wireless Communications*, vol. 27, no. 6, pp. 146–151, December 2020.

[14] L. Sixian, D. Bin, M. D. Renzo, T. Meixia, and Y. Xiaojun, "Robust secure UAV communications with the aid of reconfigurable intelligent surfaces," *arXiv:2008.09404*, 2020.

[15] Q. Wu, S. Zhang, B. Zheng, C. You, and R. Zhang, "Intelligent reflecting surface aided wireless communications: A tutorial," *IEEE Transactions on Communications*, pp. 1–1, 2021.

[16] L. Yang, F. Meng, J. Zhang, M. O. Hasna, and M. D. Renzo, "On the performance of RIS-assisted dual-hop UAV communication systems," *IEEE Transactions on Vehicular Technology*, vol. 69, no. 9, pp. 10 385–10 390, Sep. 2020.

[17] L. Yang, W. Guo, and I. S. Ansari, "Mixed dual-hop FSO-RF communication systems through reconfigurable intelligent surface," *IEEE Communications Letters*, vol. 24, no. 7, pp. 1558–1562, July 2020.

[18] A. M. Salhab and L. Yang, "Mixing RIS-assisted sources with FSO link," *arXiv:2011.05612*, 2020.

[19] P. A. O. Kehinde O. Odeyemi and O. O. Olakanmi, "Performance analysis of reconfigurable intelligent surface assisted underwater optical communication system," progress in electromagnetics research m, vol. 98, 101-111, 2020." *Progress In Electromagnetics Research M*, vol. 98, pp. 101–111, 2020.

[20] S. Li, L. Yang, D. B. da Costa, M. D. Renzo, and M.-S. Alouini, "On the performance of RIS-assisted dual-hop mixed RF-UWOC systems," *arXiv:2011.09060*, 2020.

[21] A. M. Salhab and L. Yang, "Interference impact on decode-and-forward relay networks with RIS-assisted source and relays," *arXiv:2011.05619*, 2021.

[22] D. Salim, M. H. Samuh, and A. M. Salhab, "Impact of interference on the performance of RIS-assisted source DF relaying networks," *arXiv:2011.05070*, 2020.

[23] K. Govindan, K. Zeng, and P. Mohapatra, "Probability density of the received power in mobile networks," *IEEE Trans. Wireless Commun.*, vol. 10, no. 11, pp. 3613–3619, Dec. 2011.

[24] N. C. Beaulieu and J. Xie, "A novel fading model for channels with multiple dominant specular components," *IEEE Wireless Commun. Lett.*, vol. 1, no. 4, pp. 54–57, Feb. 2015.

[25] I. S. Gradshteyn and I. M. Ryzhik, *Table of Integrals, Series, and Products*, 7th ed. Academic Press, California, 2007.

$$f_Z(z) = \frac{Az^{\frac{1}{2}(m-1)}}{2\alpha} \sum_{\ell=1}^{n} \frac{B_\ell}{D^{\beta_\ell+1}} \int_{D^{-\alpha}}^{\infty} y^{-\frac{1}{2}(m-1)-\frac{1}{\alpha}(\beta_\ell+1)-2} \exp\left(-\frac{mz}{\Omega} y^{-1}\right) I_{m-1}\left(\frac{2m\lambda\sqrt{z}}{\Omega} y^{-\frac{1}{2}}\right) \mathrm{d}y \tag{61}$$

$$f_Z(z) = \frac{A}{2\alpha} \sum_{\ell=1}^{n} \sum_{l=0}^{p} \frac{B_\ell}{D^{\beta_\ell+1}} C(l,p,m-1) \left(\frac{m\lambda}{\Omega}\right)^{m+2l-1} z^{m+l-1} \int_{0}^{D^\alpha} u^{m+l+\frac{1}{\alpha}(\beta_\ell+1)-1} \exp\left(-\frac{mz}{\Omega} u\right) \mathrm{d}u \tag{63}$$

$$f_Z(z) = \frac{1}{\alpha} \exp\left(-\frac{m\lambda^2}{\Omega}\right) \sum_{\ell=1}^{n} \sum_{l=0}^{p} \frac{B_\ell}{D^{\beta_\ell+1}} C(l,p,m-1) \lambda^{2l} \left(\frac{m}{\Omega}\right)^{l-\frac{1}{\alpha}(\beta_\ell+1)} z^{-\frac{1}{\alpha}(\beta_\ell+1)-1} \gamma_{\text{inc}}\left(m + l + \frac{1}{\alpha}(\beta_\ell+1), \frac{mD^\alpha}{\Omega} z\right) \tag{64}$$

[26] A. Olutayo, J. Cheng, and J. F. Holzman, "A new statistical channel model for emerging wireless communication systems," *IEEE OJ-COMS*, vol. 1, pp. 916–926, 2020.

[27] A. P. Prudnikov, Y. A. Brychkov, and O. I. Marichev, *Integrals and Series: Direct Laplace Transforms*. Gordon & Breach Sci. Publ., New York, 1992, vol. 4.

[28] A. P. Prudnikov *et al.*, *Integrals, and Series: More Special Functions*. Gordon & Breach Sci. Publ., New York, 1990, vol. 3.

[29] N. T. Hai and S. B. Yakubovich, *The Double Mellin–Barnes Type Integrals and Their Applications to Convolution Theory*. World Scientific Publishing Co. Pte. Ltd., 1992, vol. 6.

[30] Z. Wang and G. B. Giannakis, "A simple and general parameterization quantifying performance in fading channels," *IEEE Trans. Commun.*, vol. 51, no. 8, pp. 1389–1398, Aug. 2003.

[31] A. Kilbas and M. Saigo, *H-Transforms: Theory and Applications (Analytical Method and Special Function)*, 1st ed. CRC Press, 2004.

[32] L.-L. Li, F. Li, and F. Gross, "A new polynomial approximation for $\mathcal{J}_\nu$ bessel functions," *Appl. Math. Comput.*, vol. 183, no. 2, pp. 1220 – 1225, Dec. 2006.

[33] F. El Bouanani and D. B. da Costa, "Accurate closed-form approximations for the sum of correlated Weibull random variables," *IEEE Wireless Commun. Lett.*, vol. 7, no. 4, pp. 498–501, Jan. 2018.